Bull. Mater. Sci. (2018) 41:96
https://doi.org/10.1007/s12034-018-1614-2

Synthesis and physico-chemical properties of a new non-centrosymmetric 2-ammoniumbenzamide trioxonitrate crystals $[C_7H_9N_2O]NO_3$

YAHYA BAHROUNI[1,2,*], NEJEH HAMDAOUI[1] and LATIFA BENHAMADA[1]

[1]Laboratory of Energy and Materials (LabEM-LR11ES34), Higher School of Sciences and Technology of Hammam Sousse, University of Sousse, Hammam Sousse 4011, Sousse, Tunisia

[2]Faculty of Sciences of Monastir, University of Monastir, Avenue of the Environment 5019-Monastir, Monastir, Tunisia

*Author for correspondence (bahrouni.yahya@yahoo.fr)

MS received 7 July 2017; accepted 21 November 2017; published online 14 July 2018

Abstract. 2-Ammoniumbenzamide trioxonitrate crystals (2-ABN) were prepared and grown at room temperature. This compound crystallizes in the orthorhombic system with non-centrosymmetric $P2_12_12_1$ space group. The unit cell dimensions are $a = 4.8900(9)$ Å, $b = 9.5541(19)$ Å, $c = 18.961(4)$ Å with $V = 885.8(3)$ Å^3 and $Z = 4$. The structure refined to a reliability R factor of 4.34%. The 2-ABN structure consists of 2-ammoniumbenzamide cations ($C_7H_9N_2O^+$) and trioxonitrate anions (NO_3^-) interconnected by hydrogen bonds originating from amine group donors [N−H···O], so as to build a three-dimensional arrangement. The crystal structure, the thermal behaviour and the IR spectroscopic studies were discussed. The optical studies reveal that the 2-ABN crystal could be a good candidate for nonlinear optical devices. The dielectric properties, real and imaginary dielectric permittivities (ε' and ε'') and dielectric loss tangent (tan (δ)), of the crystal at different frequencies of the applied field are reported.

Keywords. Hybrids; X-ray diffraction; infrared spectroscopy; optical properties; dielectrics.

1. Introduction

Nonlinear optics (NLO), the technology of the 21st century, is a new domain of science and technology that plays an important role in the emerging technology of photonics. Nonlinear optical processes provide the key functions of optical switching and frequency conversion [1]. NLO materials have innumerable potential applications in laser technology, optical switching, optical communications, optical mixing, electro-optic applications and data storage [2,3]. Hence, material scientists show a considerable attention to study new types of NLO materials, which were built from organic–inorganic hybrid compounds. This hybrid compounds have the combined advantages of high optical nonlinearity and chemical flexibility of organic materials with the favourable mechanical and thermal stabilities of inorganic materials.

Nitric acid forms interesting compounds with organic cations. Recent works have led to the development of many crystals belonging to nitrates salts. Among crystals that contain nitrate anions, the most important are those, which are non-centrosymmetric because of their nonlinear optical properties [4].

In this study, we report the dielectric and optic properties of a new hybrid organic–inorganic non-centrosymmetric compound of nitrate suitable for nonlinear optical applications.

2. Experimental

2.1 *Chemical preparation*

Single crystals of 2-ABN were grown by the slow evaporation solution technique. 2-Aminobenzamide dissolved in ethanol was slowly added to nitric acid under stirring and mixed well. The solution was allowed to evaporate, after suction filtration at room temperature for a few days, until transparent crystalline salts of 2-ABN were formed. The crystals are stable under normal conditions of temperature and humidity. The reaction scheme involved in the formation of complex compound is:

$$C_7H_8N_2O + HNO_3 \xrightarrow{EtOH} (C_7H_9N_2O)NO_3.$$

2.2 *Single crystal X-ray diffraction*

Single crystal X-ray diffraction measurements were carried out at 293 K on a Nonius Kappa-CCD diffractometer using monochromated MoKα radiation. For the crystal, 90 frames were recorded, each being of 28 in φ and 60 s duration. Each frame is doubled to eliminate the uncertain electronic impulses. The first 10 frames were used for indexing reflections using the DENZO package and refined to obtain final cell parameters. Preliminary photographs indicated orthorhombic

Table 1. Crystal data and structure refinement.

Formula/formula weight	$C_7H_9N_3O_4$/199.17 g mol^{-1}
Crystal system	Orthorhombic
Space group/Z	$P2_12_12_1$(19)/4
Unit cell parameters	$a = 4.890(1)$ Å
	$b = 9.554(2)$ Å
	$c = 18.961(4)$ Å
Volume	885.8(3) Å^3
Density (calculated) (g cm^{-3})	1.493
Absorption coefficient, μ (mm^{-1})	0.124
F (0 0 0)	416
Size (mm)/colour	$0.4 \times 0.2 \times 0.15$/colourless
Diffractometer, scan mode	Kappa CCD Nonius, ϕ
Monochromator	Graphite
Wavelength	MoKα ($\lambda = 0.71073$ Å)
Theta range	$2.2 - 26.3°$
h,k,l range	$-6 =< h =< 5$
	$-11 =< k =< 11$
	$-23 =< l =< 23$
Number of independent reflections	1793
Number of reflections observed	1372
Structure resolution	Direct method: SHELXS-97
Structure refinement	Based on F2: SHELXL-97
No. of refined parameter	163
Goodness-of-fit on F^2	1.039
$R(F^2 > 2s(F^2))$ (anisotropic)/wR (F^2)	0.0434/0.1013
$\Delta\rho_{min}/\Delta\rho_{max}$ (eÅ^{-3})	−0.16/0.16
Flack parameter	0.4(10)
$w = 1/(\sigma^2(F_o^2) + (0.048P)^2 + 0.0664P)$, where $P = (F_o^2 + 2F_c^2)/3$	

symmetry and systematically absent reflections showed the space group as $P2_12_12_1$.

The structure was solved with a direct method using the SHELXS-97 programmes [5], which allows the location of the organic and NO_3 groups. The remaining non-hydrogen atoms were located by the successive difference Fourier maps using the SHELXL-97 programmes [5]. In the final least-squares refinement of atomic parameters with isotropic thermal factors of H-atoms, R decreased to 4.34% ($R_w = 10.13\%$) for 2-ABN. The basic crystallographic data and the details of the measurement and refinement are summarized in table 1. The final atomic coordinates and thermal parameters are reported in table 2.

Table 2. Final atomic coordinates and equivalent temperature factors for $(C_7H_9N_2O)NO_3$.

Atom	x	y	z	U_{iso}
C1	0.4581(6)	0.5823(3)	0.85840(16)	0.0348(7)
C2	0.2637(6)	0.4638(3)	0.86879(15)	0.0317(7)
C3	0.1963(6)	0.3726(3)	0.81363(14)	0.0319(7)
C4	0.0093(7)	0.2665(3)	0.82258(19)	0.0425(8)
C5	−0.1191(8)	0.2488(4)	0.88707(18)	0.0474(9)
C6	−0.0558(7)	0.3374(4)	0.94220(19)	0.0467(9)
C7	0.1318(7)	0.4428(3)	0.93324(17)	0.0401(8)
N2	0.5611(7)	0.6454(3)	0.91454(16)	0.0449(8)
N3	0.3189(7)	0.3864(3)	0.74330(13)	0.0384(7)
O4	0.5196(6)	0.6214(2)	0.79770(11)	0.0540(7)
N1	0.1690(6)	0.9243(3)	0.89262(14)	0.0426(7)
O1	0.1581(6)	0.9214(4)	0.82695(12)	0.0717(9)
O2	−0.0209(6)	0.8773(3)	0.92731(15)	0.0743(9)
O3	0.3698(7)	0.9735(3)	0.92035(17)	0.0905(11)

2.3 *Infrared spectroscopy*

The functional groups were identified by Fourier transform infrared (FTIR) studies at room temperature using Biored

FTS 6000 FTIR spectrometer in the range of 400–4000 cm^{-1} following KBr pellet technique. Thin transparent pellets were made by pressing the intimate mixture obtained by shaking 2 mg of the samples in 100 mg of KBr.

2.4 *UV–Vis spectral analysis*

To determine the transmission range and therefore, to know the ability of crystals for optical applications, the UV–Vis–NIR spectra of 2-ABN in liquid form (dissolved in deionized water) was recorded using a spectrophotometer in the range of 200–800 nm.

2.5 *Thermal behaviour*

The thermogravimetric and differential thermal analysis (TG/DTA) measurements of 2-aminobenzamide nitrate were carried out between 27 and 400°C in open air at a scanning rate of 10°C min^{-1} using SetaramLabsysEvo TG/DSC (1600°C) instrument.

2.6 *Dielectric measurement*

Dielectric parameters were measured on silver-electroded pellet sample in a wide frequency range at different temperatures in the range of 297–367 K at an input signal of 20 mV using PSM-1735 LCR meter.

3. Results and discussion

3.1 *Structure description*

The title compound 2-ABN ($(C_7H_9N_2O)NO_3$) has an orthorhombic geometry belonging to the space group $P2_12_12_1$ and has four formula units per unit cell. The asymmetric molecular structure is shown in figure 1.

A view of the structure projected along the $\vec{a}$ direction (figure 2) shows that the structure consists of 2-ammoniumbenzamide cations $(C_7H_9N_2O)^+$ and nitrate anions (NO_3^-) connected by hydrogen bonds. The interaction of the nitric acid with the organic molecule ($C_7H_8N_2O$) leads to the protonation of nitrogen of the amine function grafted on the benzene ring and the formation of the $(C_7H_9N_2O)^+$ cation. With regard to the organic cations arrangement, the $(C_7H_9N_2O)^+$ groups form chains, which are deployed in zigzag fashion along the $\vec{b}$ axis. The nitrate anions are intercalated between the organic cations and are deployed on corrugated form along the $\vec{b}$ axis.

The bonding angles in the nitrate anion range from 118.5(4) to 121.7°(3) and the bonding lengths have values of 1.209(4), 1.223(4) and 1.247(3) Å (table 3). These values are comparable to the reported data [6,7]. The lengthening of the N1–O1 and N1–O2 bonds is apparently caused by the connection of the O1 and O2 atoms in a system of hydrogen bonds [6] (table 4). The whole nitrate group is almost ideally planar, and the maximum deviation from the plane is equal to 0.002 Å (atom N1) (table 5).

Since protonation is performed on the nitrogen of the amine function, this is the last important function in the 2-ammoniumbenzamide cation. The bonding angles in the NH_3^+ group lie in the range of 103–114°. The deflection from the expected values for tetrahedral angles is apparently due to non-equivalent participation of all hydrogen atoms of these groups in the hydrogen bond system of the N–H···O type (table 4). Similarly, as for anilinium nitrate and mono-L-alaninium nitrate compounds, all the protons of the positively charged NH_3 group participate in the above-mentioned hydrogen bonds [6].

Hydrogen bonding play an important role in the linking of the organic cations with anions of nitrate. This interaction contributes to the cohesion of the structure. This

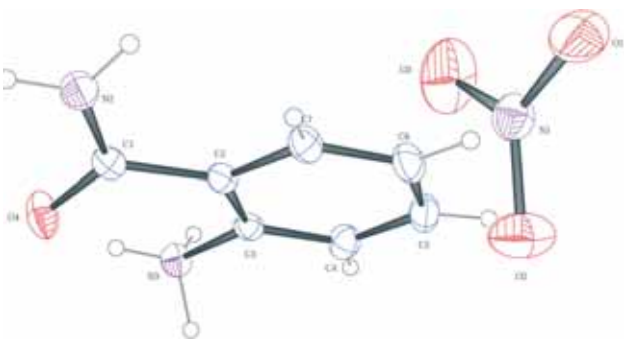

Figure 1. Asymmetric molecular structure of $(C_7H_9N_2O)NO_3$.

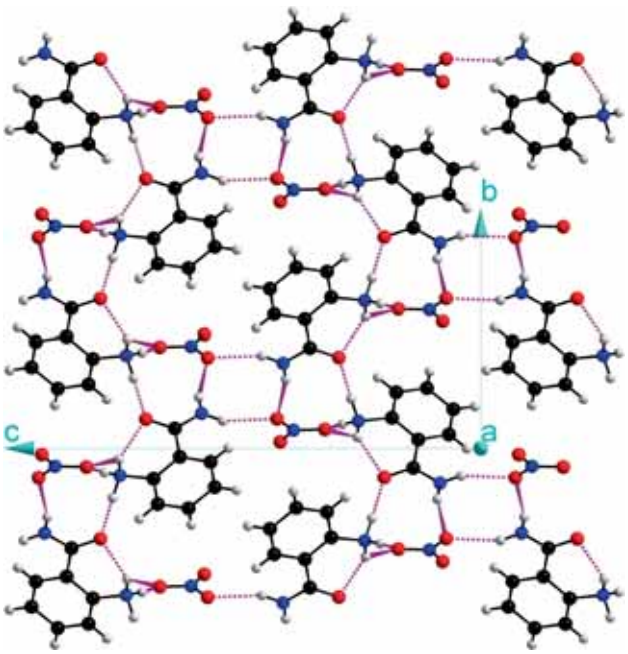

Figure 2. Projection along the $\vec{a}$ axis of the atomic arrangement in $(C_7H_9N_2O)NO_3$.

Table 3. Main interatomic distances (Å) and bond angles (○) in the $(C_7H_9N_2O)NO_3$.

N1	O1	O2	O3
O1	1.247°(3)	119.8°(3)	118.5°(4)
O2	2.137°(4)	1.223°(4)	121.7°(3)
O3	2.111°(4)	2.124°(4)	1.209°(4)
Bond lengths		Bond angles	
N2–C1	1.323(4)	C1–N2–H1N2	119(3)
N2–H1N2	0.87(5)	C1–N2–H2N2	123(3)
N2–H2N2	0.90(5)	H1N2–N2–H2N2	117(3)
N3–C3	1.468(4)	C3–N3–H1N3	109(2)
N3–H1N3	1.01(4)	C3–N3–H2N3	104(2)
N3–H2N3	1.04(5)	C3–N3–H3N3	112(3)
N3–H3N3	0.86(4)	H1N3–N3–H2N3	103.3(3)
		H1N3–N3–H3N3	114(4)
		H2N3–N3–H3N3	114(3)
C1–O4	1.247(4)	O4–C1–N2	121.0(3)
		O4–C1–C2	120.2(3)
		N2–C1–C2	118.8(3)
C2–C1	1.491(4)	C7–C2–C3	117.1(3)
C2–C7	1.396(4)	C7–C2–C1	121.3(3)
		C3–C2–C1	121.6(3)
C3–C2	1.401(4)	C4–C3–C2	121.5 (3)
C3–C4	1.376(4)	C4–C3–N3	116.7(3)
		C2–C3–N3	121.8(3)
C4–C5	1.385(5)	C3–C4–C5	120.0(3)
C4–HC4	0.96(4)	C3–C4–HC4	120.0
		C5–C4–HC4	120.0
C5–C6	1.380(5)	C6–C5–C4	119.5(3)
C5–HC5	0.90(4)	C6–C5–HC5	120.3
C6–HC6	0.98(4)	C4–C5–HC5	120.3
C7–C6	1.372(5)	C7–C6–C5	120.4(3)
C7–HC7	0.92(3)	C7–C6–HC6	119.8
		C5–C6–HC6	119.8
		C6–C7–C2	121.5(3)
		C6–C7–HC7	119.2
		C2–C7–HC7	119.2

atomic arrangement exhibits N−H···O type of intermolecular interaction, classified as strong and weak hydrogen bonds. Indeed, the O1 oxygen of the nitrate group participates in both strong and weak hydrogen bonds by connecting H2 and H3 of the same NH_3^+ group in the order of 1.69 and 2.39 Å, respectively. The O_2 oxygen connect to the N_2 atom of two different organic cations via two weak hydrogen bonds, N2–H1N2···O2 and N2–H2N2···O2, in the order of 2.18 Å. For this reason,

Table 4. Bond lengths (Å) and angles (○) in the hydrogen-bonding scheme[a] of $(C_7H_9N_2O)NO_3$.

	D–H	H···A	D···A	D−H···A
N3−H1N3···O4(i)	1.01(4)	1.76(4)	2.764(4)	172(4)
N3−H2N3···O1(ii)	1.04(5)	1.69(5)	2.707(4)	168(4)
N2−H2N2···O2(iii)	0.9(5)	2.18(5)	3.033(5)	159(4)
N2−H1N2···O2(iv)	0.87(5)	2.18(5)	3.025(5)	164(4)
N3−H3N3···O4	0.86(4)	1.97(4)	2.658(4)	136(3)
N3−H3N3···O1(i)	0.86(4)	2.39(4)	2.903(4)	119(3)

[a]Equivalent positions: (i) $-x+1$, $y-1/2$, $-z+3/2$, (ii) $-x$, $y-1/2$, $-z+3/2$, (iii) $x+1/2$, $-y+3/2$, $-z+2$, (iv) $x+1$, y, z.

Table 5. Analysis of the planarity[a] of nitrate group.

Atom	Atomic deviations (Å)
N1	0.002(3)
O1	−0.0006(9)
O2	−0.0006(9)
O3	−0.0006(9)

[a]Equation of the plane: $-2.1196(0.0092)x+8.6099(0.0089)y+0.0055(0.0414)z = 7.6034(0.0388)$.

the O1 atom owns the largest N–O bonding length. In addition, each cation is associated with another cation with strong hydrogen bonds N3–H1N3···O4, and produce one intra-hydrogen bonding N3–H3N3···O4, which spread within the respective ranges: 1.76 and 1.97 Å.

3.2 *Infrared spectroscopy*

The infrared FTIR spectrum of 2-ABN single crystals scanned between 400 and 4000 cm^{-1} is shown in figure 3. The recorded FTIR spectra were compared with the standard spectra of the functional groups.

3.2a *Internal vibrations of NO_3^- anions*: Assignment of the bands in the vibrational spectra of 2-ammoniumbenzamide trioxonitrate was based on the results of a previous study on the interpretation of the vibrational spectra of nitrate.

The planar NO_3^- free ion (D_{3h}) has six vibrational degrees of freedom. They form four fundamental modes: symmetric stretching (ν_1) occur at 1049 cm^{-1} (Raman active) and an out-of-plane bending (ν_2) at 830 cm^{-1} (IR active). Furthermore, an antisymmetric stretching (ν_3) can be reasonably assigned to the bands at 1355 cm^{-1} (doubly degenerated, both IR and Raman active) and a plane bending vibrations (ν_4) appear at 690 cm^{-1} (doubly degenerated, both IR and Raman active) [8].

For the compound under study, the nitrate anion is not totally free. It is attached to the 2-aminobenzamide cation.

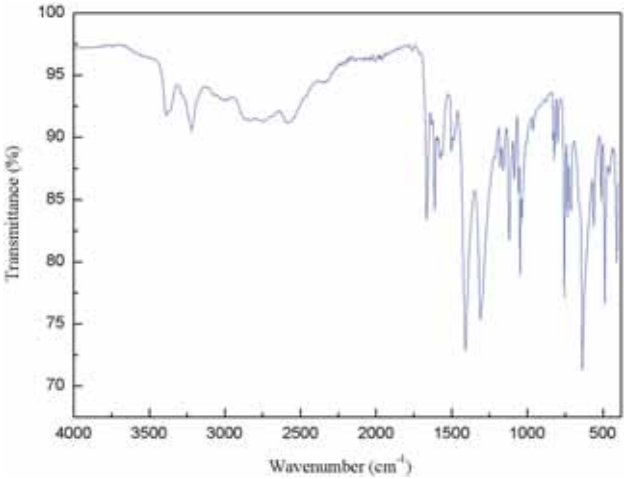

Figure 3. IR spectrum of $(C_7H_9N_2O)NO_3$.

The oxygen of nitrate group is involved in the hydrogen bonding with the hydrogen of the NH_3^+ group and NH_2 of amide function.

The presence of nitrate anions in the title compound can be confirmed by the presence of characteristic vibrations arising due to N–O vibrations. Really, the peak at 1034 cm^{-1} corresponds to the symmetric stretching mode (ν_1 mode). Here, the excitation of the IR-inactive mode is due to the local crystalline environment [8,9]. The weak peaks at 821 and 828 cm^{-1} are assigned to the ν_2, the symmetric bending mode. The splitting of this mode into a doublet may be ascribed to a lowering of symmetry of NO_3^- ion from D_{3h} to C_{2v} or C_s due to the hydrogen bond formation [7]. The asymmetric stretching mode appears as a strong peak at 1309 cm^{-1}. This feature is comparable to the behaviour of L-ornithine nitrate and DL-phenylalaninium nitrate [8,9]. The in-plane bending mode of vibration ν_4, which is doubly degenerated, forms weak peaks doublet at 734 and 712 cm^{-1}. This is similar to DL-phenylalaninium nitrate [8].

The stretching wavenumbers are slightly lower and the bending wavenumbers are slightly higher than those expected for the free ion state due to hydrogen bonding [9].

3.2b *NH_3^+ group vibrations*: The second important functional group is the ammonium group NH_3^+. In the free state, it has C_{3v} symmetry with a pyramidal structure. The normal modes of vibrations are $\nu_1(A_1)$, $\nu_2(A_2)$, ν_3 (E) and ν_4 (E). All these four modes of vibrations are both IR and Raman active.

The symmetric stretching (ν_1) and bending modes (ν_2) are non-degenerated, but the asymmetric stretching (ν_3) and bending modes (ν_4) are doubly degenerated. In the compound under study, the X-ray data reveals that each of the three hydrogen atoms in the NH_3^+ participates in hydrogen bonding. As the NH_3^+ ion is attached, the N–H bond is weakened and there will be a shift in the vibrational wavenumbers. Hydrogen bonding is responsible for shifting the deformation modes to higher wavenumbers and lowering the stretching wavenumbers [8].

In primary amine salt containing the NH_3^+ group bending modes, which are asymmetric and symmetric deformation modes, are expected to appear at 1600–1575 and 1550–1504 cm^{-1}, respectively, whereas the asymmetric and symmetric stretching modes of this group appear in the region of 2800–3000 cm^{-1}. In the present investigation, the bands between 2840 and 2580 cm^{-1} in the IR spectrum is assigned to the stretching vibrations of the NH_3^+ group. The doubly degenerated asymmetric deformation vibration of this group is observed as a medium peak at 1617 cm^{-1}. However, the symmetric deformation mode is observed as a medium intensity line at 1577 cm^{-1}. The C–N out-of-plane bending mode of vibration lies in the expected region. It occurs at 488 and 512 cm^{-1}.

3.2c *Vibrations of the amide function*: The asymmetric and symmetric stretching modes of the NH_2 group of amide function were identified together with its deformation mode. They are expected to appear at 3350–3475 and 3385–3160 cm^{-1}, respectively. For the compound under study, the asymmetric stretching mode of the NH_2 group is observed at 3388 cm^{-1}, whereas the N–H symmetric stretching vibration appears around 3219 cm^{-1}.

Regarding the deformation mode, the strong band at 636 $cm^{-1}$is assigned to the N–H waging mode, as expected, while, the rocking mode is observed as a medium band at 1120 cm^{-1}. Among the characteristic bands of the amide function, we found the vibration of C–N and C=O bonds. Definitely, the C–N and C=O stretching modes are observed at 1409 and 1665 cm^{-1}, respectively.

3.2d *Aromatic vibrations*: The 2-ammoniumbenzamide trioxonitrate crystal has an ortho-disubstituted phenyl. The stretching and bending frequencies of this aromatic ring are observed in the expected region [7]. Certainly, the hydrocarbon C–H stretch occurs near 3000 cm^{-1}. For the C–H out-of-plane bending mode, the band appears at 756 cm^{-1}, while, the aromatic in-plane C–H bending absorbs at 1084 cm^{-1}. The presence of C=C stretching vibrations of the aromatic ring is consistent with the absorption bands at 1500 and 1488 cm^{-1}.

3.3 *UV–Vis spectral analysis*

The UV–Vis spectrum provides structural information because the absorption of UV and visible light involves the promotion of the electrons in σ and π orbitals from the ground state to higher energy states [10,11]. The optical transmission is very important to identify the potential of the NLO material, because the material can be of utility only if it has wide transparency window and reduced absorption around the fundamental and second-harmonic wavelength [12,13].

The spectrum of absorbance showed that this compound absorbs between 220 and 361 nm with a maximum absorption

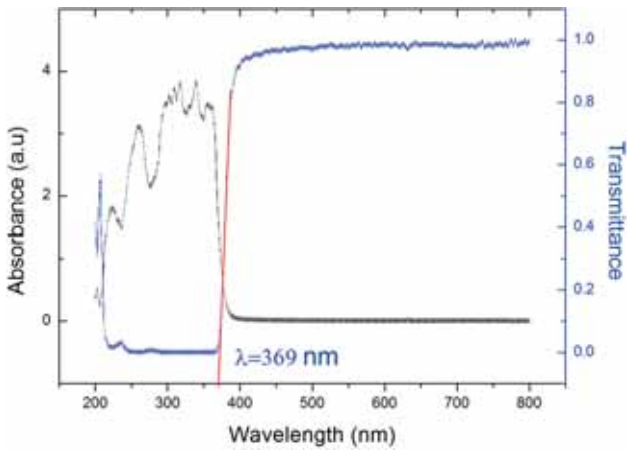

Figure 4. UV–Vis and optical transmittance spectra of 2-ABN.

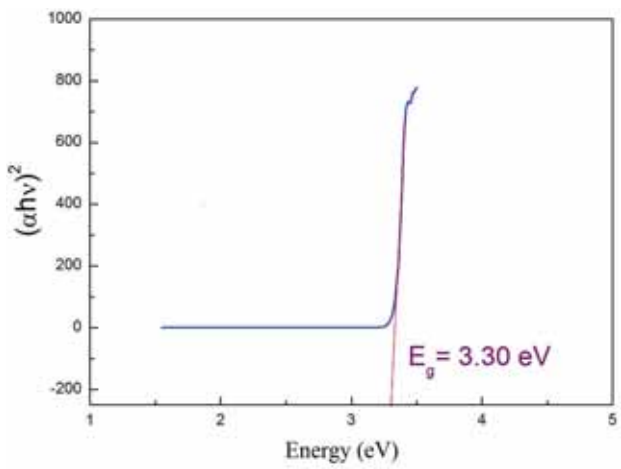

Figure 5. Plot of $(\alpha h\nu)^2$ *vs*. photonenergy of 2-ABN crystal.

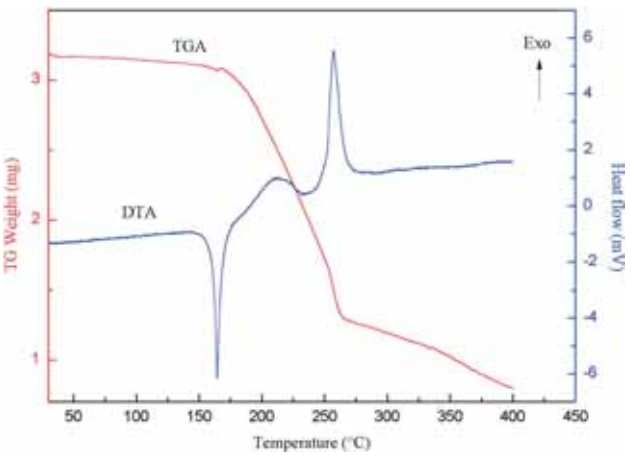

Figure 6. TG–DTA thermograms of 2-ABN.

(λ_{max}) at 339. Furthermore, the transmission spectrum shows that the lower ultraviolet cutoff of the crystal occurs at 369 nm and there is no remarkable absorption in the entire region of the spectra (figure 4). The title compound has a transmittance of about 95% from 394 to 800 nm. The transmission window in the visible region enables good optical transmission of the second-harmonic frequencies.

The energy band gap of the crystal is determined from the transmittance spectra using the relation [14]:

$$(\alpha h\nu)^2 = A\left(h\nu - E_g\right), \tag{1}$$

where A is a constant, h the Planck's constant, ν the photon frequency, E_g the band gap of the material, α the absorption coefficient, which is calculated from the equation:

$$\alpha = \frac{2.3026 \times \text{Abs}}{d}, \tag{2}$$

where Abs is the absorbance of the material and d the path length (1 cm).

The Tauc's plot between $(\alpha h\nu)^2$ and $h\nu$ is shown in figure 5. The band gap of 2-ABN was found as 3.30 eV, it was obtained by the interception of the extrapolated straight line of the linear part with the x-axis. This value is so close to the one calculated using the cut-off wavelength ($E_g = 3.36$ eV) using the following formula:

$$E_g = \frac{h\nu}{\lambda_{\text{cut-off wavelength}}}. \tag{3}$$

The broad optical band gap of 2-ABN crystals confirms the vast transmittance in the visible region.

3.4 *Thermal behaviour*

The TG/DTA thermogram of the 2-ABN is illustrated in figure 6. The DTA curve of the crystal reveals that no endothermic/exothermic peak is observed below 165°C, suggesting its structure is stable in the respective region. In addition, the thermogravimetric analysis (TGA) thermogram shows that there is no weight loss in the respective region. Hence, the crystal is devoid of any entrapped or physically adsorbed water. This stability ensures the suitability of the material for possible application in lasers, where the crystal is required to withstand high temperatures [15].

A major weight loss starting at about 165°C is observed from the TGA trace. The decomposition completes at about 400°C leaving no residue. The endothermic peak in the DTA curve at 165°C represents the melting point of the sample, and the exothermic peak appearing at 257°C indicates the combustion of the compound.

3.5 *Dielectric studies*

The dielectric permittivity, $\varepsilon_r = \varepsilon_r' - i\varepsilon_r''$, is the most important characteristic of the dielectric properties of a material. The real part of the permittivity (ε_r') expresses the energy deposited in the sample, while the imaginary part (ε_r'') expresses the

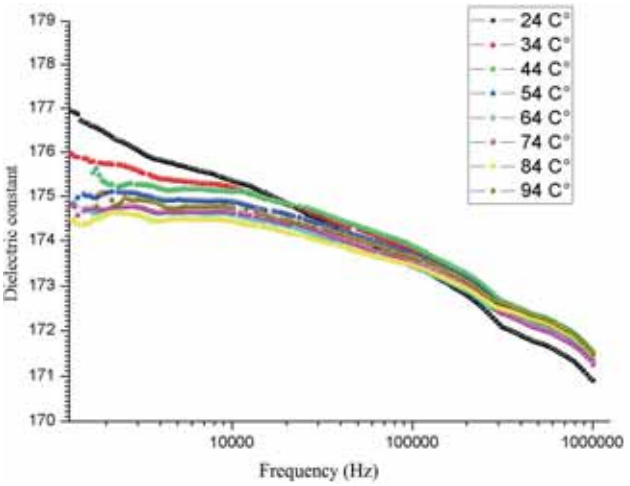

Figure 7. Dielectric constant curves with frequency for 2-ABN single crystals at different temperatures.

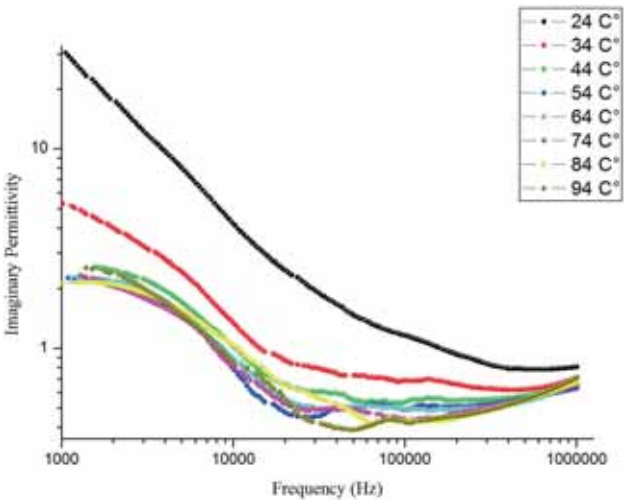

Figure 8. Dielectric permittivity curves with frequency for 2-ABN single crystals at different temperatures.

energy spent for the molecular motion, i.e., dissipation electric field's energy.

The frequency dependence at some selected temperatures of the real permittivity ε'_r is presented in figure 7. At low frequencies, the high value of ε'_r may be attributed to the existence of all the four polarizations namely, orientational, space charge, ionic and electronic polarizations. In addition, the decrease in the dielectric permittivity with the frequency of the sample under the study may be essentially due to the decreasing number of dipoles, which participates to polarization or either to the inability of dipoles to rotate rapidly leading to a lag between frequency of oscillating dipole and that of applied field. The nature of the real permittivity related to oscillating free dipoles in an alternating field may be described as follows: the dipoles follow the field for frequencies $\omega << 1/\tau$, where τ is the relaxation time. As frequency increases ($\omega < 1/\tau$), the dipoles begin to lag behind the field and ε'_r decrease slightly. The real permittivity shows relaxation process when frequency attains a characteristic value ($\omega = 1/\tau$). At sufficiently high frequencies $\omega >> 1/\tau$, the dipoles can no longer follow the field and $\varepsilon'_r \approx \varepsilon_\infty$ (high frequency value of ε'_r).

Figure 8 represents the frequency dependences of the imaginary part of the permittivity of the investigated compound at fixed temperatures. In the high frequency range, the dielectric spectra present a quasi-Debye-type behaviour and a strong deviation from the Debye-type behaviour at lower frequencies, which implicates a complicated expression. The imaginary part of the complex permittivity [16] is:

$$\varepsilon''_r(\omega) = \frac{(\varepsilon_s - \varepsilon_\infty)(\omega/\omega_1)^{1-\alpha}\sin((1-\alpha)\pi/2)}{1 + 2(\omega/\omega_1)^{1-\alpha}\cos((1-\alpha)\pi/2) + (\omega/\omega_1)^{2(1-\alpha)}} + \frac{\sigma_0}{\varepsilon_0\omega}, \quad (4)$$

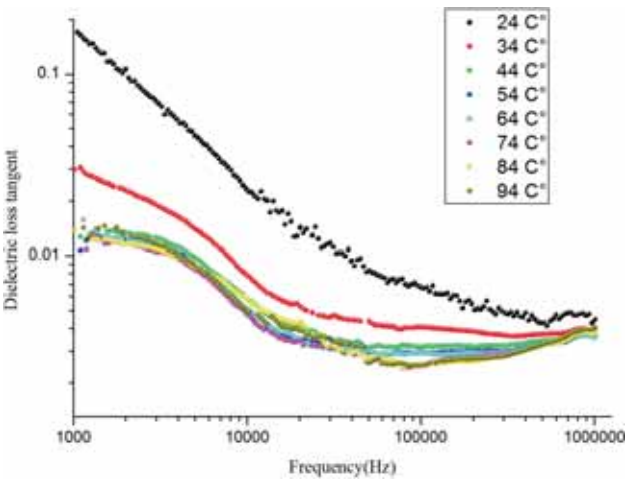

Figure 9. Dielectric loss curves with frequency for 2-ABN single crystals at different temperatures.

where α represents the tilting angle ($\alpha\pi/2$) of the circular arc from the real axis in the complex permittivity plan, ω the frequency, σ_0 the specific conductivity, ε_s the static permittivity, ω_1 the relaxation angular frequency of the Debye process and ε_0 the dielectric permittivity of vacuum. The first part in equation (4) is related to the thermal polarization and the second one to the electrical conductivity. The rising of the imaginary part of the permittivity at low frequency indicates that electrode polarization and space charge effects have existed confirming non-Debye dependence [17]. In this study, there are no significant relaxation peaks in the frequency range, only a tail related to the conductivity was observed.

As shown in figure 9, the dielectric loss tangent is studied at different temperatures as a function of frequency. These curves indicate that the dielectric loss depends on the frequency of the applied field. The dielectric loss decreases as

the frequency increases. Furthermore, the fall of loss as frequency is lesser and as the temperature increases. The low dielectric loss at higher frequency of the compound under study proposes that the compound has good optical quality with lesser traps and this parameter of crucial importance for nonlinear optical materials in their applications [18].

4. Conclusion

A non-centrosymmetric material, $(C_7H_9N_2O)NO_3$, with $P2_12_12_1$ space group symmetry was prepared and structurally characterized. The grown crystal was confirmed by XRD analysis. The functional groups of the 2-ABN crystal were identified by the FTIR analysis. The good transmission property of the crystal in the entire visible region ensures its suitability for SHG applications. The thermal analysis reveals that the grown crystal is stable up to 165°C. The low value of dielectric constant and dielectric loss at higher frequencies suggests that the crystals possess enhanced optical quality, which has significant role in the NLO applications.

Acknowledgements

This work was supported by the Ministry of Higher Education and Scientific Research of Tunisia.

References

[1] Saravana K G and Murugakoothan P 2014 *Spectrochim. Acta A* **131** 17
[2] Pal T, Kar T, Bocelli G and Rigi L 2003 *Cryst. Growth Des.* **3** 13
[3] Penn B G, Cardelino B H, Moore C E, Shields A W and Frazier D O 1991 *Prog. Cryst. Growth Charact. Mater.* **22** 19
[4] Bouchouit K, Sofiani Z, Derkowska B, Abed S, Benali-Cherif N, Bakasse M *et al* 2007 *Opt. Commun.* **278** 180
[5] Sheldrick G M 2008 *Acta Cryst. A* **64** 112
[6] Němec I, Gyepes R and Mička Z 1999 *J. Mol. Struct.* **476** 203
[7] Marchewka M K and Pietraszko A 2005 *J. Phys. Chem. Solids* **66** 1039
[8] Briget Mary M, Sasirekha V and Ramakrishnan V 2005 *Spectrochim. Acta A* **62** 446
[9] Ramaswamy S, Umadivi M, Rajaram R K and Ramakrishnan V 2003 *J. Raman Spectrosc.* **34** 806
[10] Masilamani S and Mohamed Musthafa A 2013 *Microchem. J.* **110** 749
[11] Sankar R, Raghavan C M, Balaji M, Mohan Kumar R and Jayavel R 2007 *Cryst. Growth Des.* **7** 348
[12] Periyasamy B K, Jebas R S and Thailampillai B 2007 *Mater. Lett.* **61** 1489
[13] Hemaraju B C, Ahlam M A, Pushpa N, Mahadevan K M and Gnana Prakash A P 2015 *J. Optik.* **151** 854
[14] Ashour A, El-Kadry N and Mahmoud S A 1995 *Thin Solid Films* **269** 117
[15] Dhanuskodi S and Vasantha K 2004 *Cryst. Res. Technol.* **39** 259
[16] Cole K S and Cole R H 1941 *J. Chem. Phys.* **9** 341
[17] Govindaraj G, Baskaran N, Shahi K and Monoravi P 1995 *Solid State Ionics* **76** 47
[18] Kanagathara N, Renganathan N G, Marchewka M K, Sivakumar N, Gayathri K, Krishnan P *et al* 2013 *Spectrochim. Acta A* **101** 112